Calibration of an interferometric on-machine probing system on an ultra-precision turning machine

Authors:

Duo Li, Zhen Tong, Xiangqian Jiang*, Liam Blunt, Feng Gao

EPSRC Centre for Innovative Manufacturing in Advanced Metrology,

Centre for Precision Technologies,

University of Huddersfield,

Huddersfield, UK, HD1 3DH

Corresponding author: Xiangqian Jiang*

Email: x.jiang@hud.ac.uk

Calibration of an interferometric on-machine probing system on an ultra-precision turning machine

Abstract

Surface measurement is fundamental to further enhance accuracy and efficiency in ultra-precision machining. Advanced on-machine measurement (OMM) is evolving as the key enabling technology for autonomous and intelligent manufacturing. The present work integrates an interferometric probing system on an ultra-precision turning machine. However, due to relatively harsh environment in the machine tools, metrology characteristics of surface measuring instrument would deviate from those tested in laboratories. In order to improve the performance of on-machine measurement system, it is necessary to calibrate the OMM system and compensate the systematic errors. Three major error sources, including on-machine vibration, machine tool kinematic errors, and linearity errors are investigated according to the characteristics of interferometric single point OMM. For on-machine vibration, a theoretical study of the relationship between sampling frequency, scanning parameters, vibration frequency and topography frequencies of interest is first presented. Static and scanning vibration tests are performed in order to select the proper sampling frequency. Machine scanning error is mapped for OMM correction with the proposed kinematic error modelling measurement and compensation method. Calibration of the response curve and linearity error correction is conducted by measuring a radially distributed step height sample on the machine. Experimental investigation is conducted which proves the validity of proposed calibration methodology and the effectiveness of OMM. After the calibration process, OMM results agree well with calibrated offline measurements.

Keywords

On-machine measurement; Measurement calibration; Non-contact; Ultra-precision turning machine

1 Introduction

Ultra-precision manufacturing has been developed over decades to produce surfaces with optical, electronic or mechanical functions for highly demanding applications [1]. Surface measurement is fundamental in providing valuable information to control the surface generation process and improving machining accuracy [2]. In order to increase the measurement efficiency in advanced manufacturing, a shift in the approach of metrology from offline lab based solutions towards the use of metrology upon manufacturing platforms is urgently needed [3-5]. The advantage of on-machine metrology is the consistent coordinate system between machining and measurement process, which avoids the errors caused by re-positioning workpieces and utilizes the machine axes to extend the measuring range [6]. However, due to the relatively harsh environment on the machine tools compared with that in the laboratory, several factors degrade measurement accuracy and need to be considered, including on-machine vibration, machine scanning motion error and environmental variations. Therefore, it is necessary to calibrate the measurement system and compensate for these systematic errors. Calibration of on-machine measurement systems for ultra-precision machining processes will enable the potential improvement of both measurement and machining accuracy.

Although the metrology characteristics of offline measurement instruments have been intensively investigated [7, 8], there is still relatively little research regarding the calibration process of OMM for ultra-precision machining. Zhu et al. [9] presented a scanning tunneling microscope for OMM of diamond machined optical micro-structured surfaces. To facilitate the reliable quantification of the demanding specifications, the author investigated modeling and analysis of uncertainty in the characterization of form error of structured surfaces. Gao et al. [10] developed an atomic force microscope (AFM) system to measure sinusoidal microstructures on a diamond turning machine. A flat standard was employed to characterize the errors of the scanning stages and compensated for measurement data. The metrology system with the proposed alignment was able to accurately measure in a spiral path with nanometre resolution. Zou et al. [11] integrated a chromatic confocal sensor on a diamond turning machine to achieve the non-contact measurement of machined components. To check the linearity precision of the confocal probe, a 50 μm quartz step height standard was mounted and measured on the machine. Quinsat and Tournier [12] employed chromatic confocal sensors on a five-axis machining centre. They evaluated the measurement performance of the integrated system. Several issues including geometric error, thermal effects and positioning repeatability were taken into consideration and compensation strategies were presented. Most studies have focused on the development and evaluation of measurement sensors characteristics. However, less attention has been paid to evaluate comprehensive performance of OMM systems and the presentation of a systematic calibration methodology. In this paper, the configuration of an OMM system and its setup are introduced. The following section will present a systematic calibration methodology of the OMM system. Three aspects will be discussed in detail, including on-machine vibration, machine kinematic error, and linearity error. Finally, a set

of calibration and OMM experiments were carried out to prove the validity of the calibration process and the effectiveness of the OMM system.

2 Methodology of calibration OMM

2.1 Overview

An in-house designed interferometric probe, termed Dispersed Reference Interferometry (DRI), is integrated onto a 3 axis ultra-precision machine (Nanoform 250, Precitech), equipped with two linear hydrostatic axes and one rotational axis. The fibre-linked compact and dynamic design allows it to operates in volume limited ultra-precision manufacturing environments, with measuring range and resolution capabilities of 800 μm and 0.6 nm respectively [13]. The system configuration is illustrated in Figure 1.

Before OMM operation, the DRI probe is aligned coaxially to the spindle rotational axis, by means of multiple scanning of a convex sphere sample. The fitted apex point can be considered as the coaxial position and is saved in the machine tool coordinate system. The selection of measurement path primarily depends on the measurement tasks and surface feature distribution. Three measurement paths (multiple radial, multiple circular and spiral) with corresponding applicable surfaces are illustrated in Figure 2.

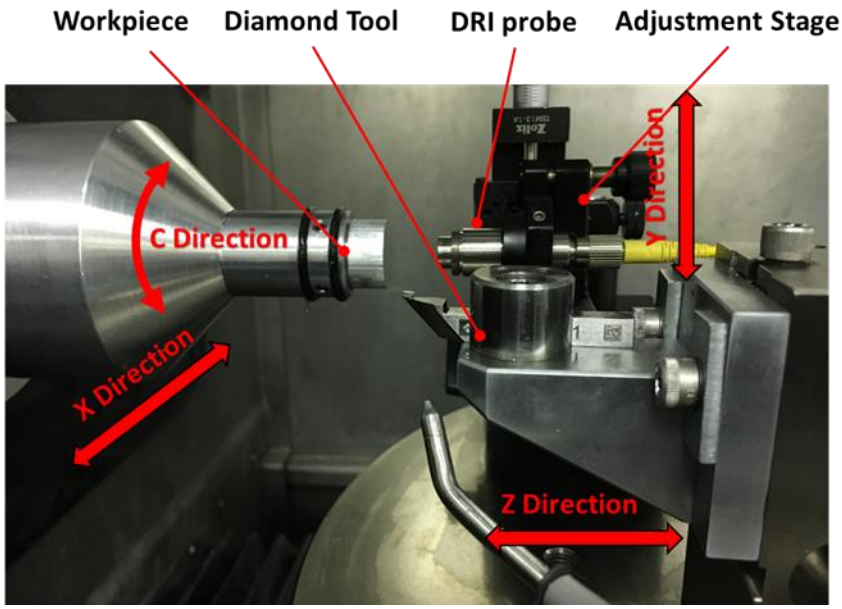

Figure 1 OMM system setup

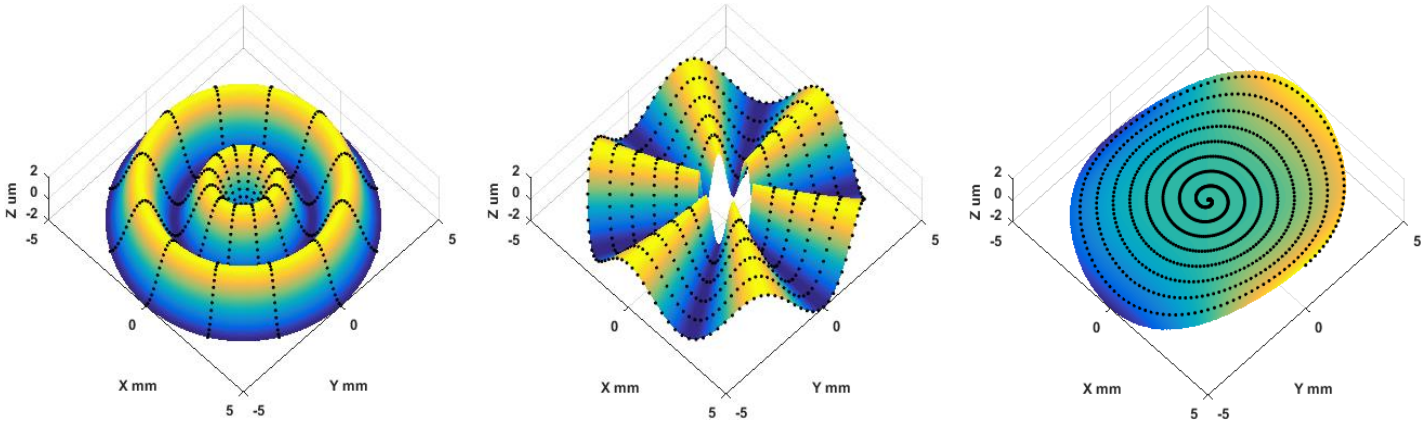

(a) Multiple radial path **(b) Multiple circular path** **(c) Spiral path**

Figure 2 Multiple radial, multiple circular, spiral measurement paths

Measuring conditions vary with machine configuration, probing system setup, measurement task and so on. Calibration of the OMM system is thus considered to be a task specific process [14]. According to the configuration and measurement task of the OMM system for the diamond turning process, the calibration process is performed in the sensitive direction (*Z* direction shown in Figure 1). The measurement accuracy in the radial scanning direction (*X* direction) is guaranteed by the ultra-precision linear scale feedback (with 8.6 nm resolution), which compares

positively with micrometre-level lateral resolution achievable in common optical instruments [15]. Thus the calibration in the lateral direction is not considered in the work. Three aspects of OMM are taken into consideration and discussed in the following sections: on-machine vibration test, machine kinematic error mapping and compensation, amplification coefficient and linearity error calibration.

2.2 On-machine vibration analysis

Aspects of the machine tool environment will inevitably influence the performance of OMM systems. Vibration from machine tool axes, such as the air bearing spindle and linear stages will degrade measurement results. Probe internal noise may also be magnified due to the electromagnetic disturbance. Therefore, it is necessary to conduct on-machine vibration testing and analysis to assess its relationship with the sampling frequency, scanning parameters and filtration operations in post processing. On-machine vibration in the measurement process is a combination of the internal noise of the instrument, machine tool static vibration and vibration induced by the machine motion. The induced vibration components onto the OMM result should be filtered out for accurate characterization of the surface form and topography.

According to Nyquist sampling theorem [16], the sampling frequency F_s is required to be at least 2 times the on-machine vibration frequency $F_{vibration}$ to avoid aliasing. Also, to separate the vibration frequency component from the frequency associated with the topography features of interest F_{topo}, the upper limit of F_{topo} is recommended to be lower than the $F_{vibration}$. The relationship between λ_{topo} and F_{topo} is described as follows:

$$\lambda_{Topo} = \frac{Feedrate}{F_{Topo}} \tag{1}$$

where λ_{topo} is the wavelength of the surface topography of interest and F_{topo} is the corresponding frequency.

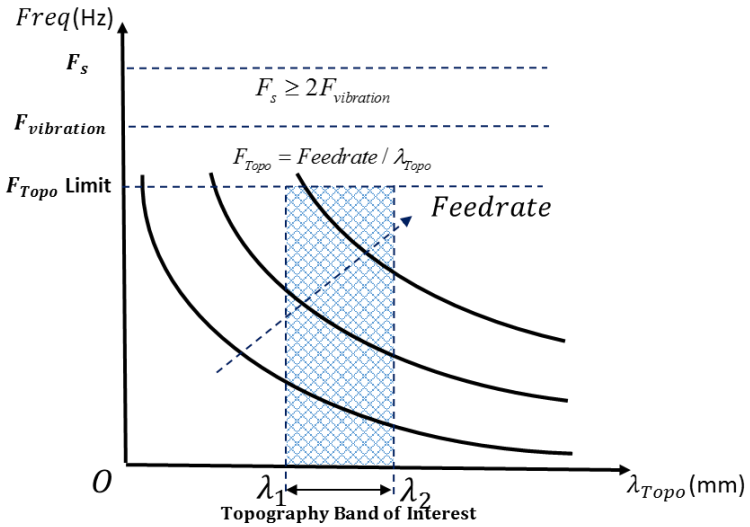

Figure 3 Sampling frequency decision graph

According to the topography band of interest and vibration test results, a frequency decision graph is plotted in Figure 3, providing guidance in selection the proper scanning parameters and sampling frequency. For a given scanning feedrate, the topography frequency of interest should be lower than the vibration frequency shown in the hatched region. To meet the requirement for avoiding signal aliasing, lower scanning speed and higher sampling frequency are preferable from the perspective of filtering out induced vibration components from the topography band of interest. However, other issues have to be carefully considered, such as computation cost and measurement efficiency.

2.3 Machine tool kinematic modelling

For on-machine surface measurement, the DRI probe is carried by the machine tool axes to cover the inspection area. Due to mechanical imperfections, wear of machine tool elements, and stage misalignments, the deviation from the programmed scanning path will induce additional measurement errors [17]. Therefore, the influence of machine tool kinematic errors on OMM results needs to be modelled, measured and compensated. Kinematic error modelling in machine tools is based on rigid body kinematic [18] and multi-body system theory [19]. Multi-body system theory offers a comprehensive description of general mechanical systems utilizing a lower order body topological structure. Using homogeneous transformation matrix (HTM), spatially distributed single error components can be synthesized as a volumetric error model. For the 3-axis turning configuration in the current work, there are two kinematic error chains shown in Figure 4. One is from machine base to the workpiece surface, and the other is from the machine base to the interferometric probe.

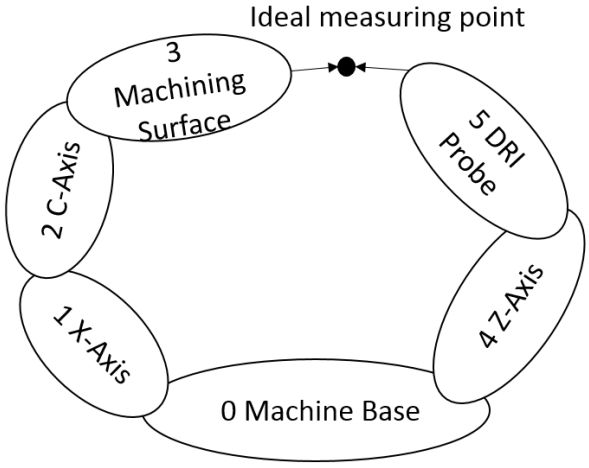

Figure 4 Error kinematic chain for OMM system

Based on rigid body kinematics, transformation matrix ${}_{k}^{j}T$ describes the coordinate transformation from coordinate *k* to coordinate *j*, which comprises four component matrices and can be formulated as:

$$ {}_{k}^{j}T = {}_{k}^{j}T_{l}\ {}_{k}^{j}T_{le}\ {}_{k}^{j}T_{m}\ {}_{k}^{j}T_{me} \tag{2} $$

where ${}_{k}^{j}T_{l}$ is the location transformation matrix, ${}_{k}^{j}T_{le}$ is the location error transformation matrix, ${}_{k}^{j}T_{m}$ is the motion (translation or rotation) transformation matrix, and ${}_{k}^{j}T_{me}$ is the motion (translation or rotation) error transformation matrix. These matrices are expressed as follows:

$$ {}_{k}^{j}T_{l} = \begin{bmatrix} 1 & 0 & 0 & p_{kx} \\ 0 & 1 & 0 & p_{ky} \\ 0 & 0 & 1 & p_{kz} \\ 0 & 0 & 0 & 1 \end{bmatrix} \tag{3} $$

where [p_{kx} , p_{ky} , p_{kz}] are the location vectors from coordinate *k* to coordinate *j*.

$$ {}_{1}^{0}T_{m} = \begin{bmatrix} 1 & 0 & 0 & x \\ 0 & 1 & 0 & 0 \\ 0 & 0 & 1 & 0 \\ 0 & 0 & 0 & 1 \end{bmatrix} \tag{4} $$

$$ {}_{4}^{0}T_{m} = \begin{bmatrix} 1 & 0 & 0 & 0 \\ 0 & 1 & 0 & 0 \\ 0 & 0 & 1 & z \\ 0 & 0 & 0 & 1 \end{bmatrix} \tag{5} $$

$$ {}_{2}^{1}T_{m} = \begin{bmatrix} cos(c) & -sin(c) & 0 & 0 \\ sin(c) & cos(c) & 0 & 0 \\ 0 & 0 & 1 & 0 \\ 0 & 0 & 0 & 1 \end{bmatrix} \tag{6} $$

$$ {}_{k}^{j}T_{me} = \begin{bmatrix} 1 & -E_{Ck} & E_{Bk} & E_{Xk} \\ E_{Ck} & 1 & -E_{Ak} & E_{Yk} \\ -E_{Bk} & E_{Ak} & 1 & E_{Zk} \\ 0 & 0 & 0 & 1 \end{bmatrix} \tag{7} $$

According to the kinematic chain structure illustrated in Figure 4, all transformation matrices between adjacent coordinate systems can be derived as follows:

$$ {}^{0}_{1}T = \begin{bmatrix} 1 & 0 & 0 & p_{1x} \\ 0 & 1 & 0 & p_{1y} \\ 0 & 0 & 1 & p_{1z} \\ 0 & 0 & 0 & 1 \end{bmatrix} \begin{bmatrix} 1 & 0 & 0 & 0 \\ 0 & 1 & 0 & 0 \\ 0 & 0 & 1 & 0 \\ 0 & 0 & 0 & 1 \end{bmatrix} \begin{bmatrix} 1 & 0 & 0 & x \\ 0 & 1 & 0 & 0 \\ 0 & 0 & 1 & 0 \\ 0 & 0 & 0 & 1 \end{bmatrix} \begin{bmatrix} 1 & -E_{CX} & E_{BX} & E_{XX} \\ E_{CX} & 1 & -E_{AX} & E_{YX} \\ -E_{BX} & E_{AX} & 1 & E_{ZX} \\ 0 & 0 & 0 & 1 \end{bmatrix} $$

(8)

$$ {}^{1}_{2}T = \begin{bmatrix} 1 & 0 & 0 & p_{2x} \\ 0 & 1 & 0 & p_{2y} \\ 0 & 0 & 1 & p_{2z} \\ 0 & 0 & 0 & 1 \end{bmatrix} \begin{bmatrix} 1 & 0 & E_{BOC} & 0 \\ 0 & 1 & -E_{AOC} & 0 \\ -E_{BOC} & E_{AOC} & 1 & 0 \\ 0 & 0 & 0 & 1 \end{bmatrix} \begin{bmatrix} \cos(c) & -\sin(c) & 0 & 0 \\ \sin(c) & \cos(c) & 0 & 0 \\ 0 & 0 & 1 & 0 \\ 0 & 0 & 0 & 1 \end{bmatrix} \begin{bmatrix} 1 & -E_{CC} & E_{BC} & E_{XC} \\ E_{CC} & 1 & -E_{AC} & E_{YC} \\ -E_{BC} & E_{AC} & 1 & E_{ZC} \\ 0 & 0 & 0 & 1 \end{bmatrix} \quad (9) $$

$$ {}^{2}_{3}T = \begin{bmatrix} 1 & 0 & 0 & p_{3x} \\ 0 & 1 & 0 & p_{3y} \\ 0 & 0 & 1 & p_{3z} \\ 0 & 0 & 0 & 1 \end{bmatrix} \quad (10) $$

$$ {}^{0}_{4}T = \begin{bmatrix} 1 & 0 & 0 & p_{4x} \\ 0 & 1 & 0 & p_{4y} \\ 0 & 0 & 1 & p_{4z} \\ 0 & 0 & 0 & 1 \end{bmatrix} \begin{bmatrix} 1 & 0 & E_{BOZ} & 0 \\ 0 & 1 & 0 & 0 \\ -E_{BOZ} & 0 & 1 & 0 \\ 0 & 0 & 0 & 1 \end{bmatrix} \begin{bmatrix} 1 & 0 & 0 & 0 \\ 0 & 1 & 0 & 0 \\ 0 & 0 & 1 & \mathrm{z} \\ 0 & 0 & 0 & 1 \end{bmatrix} \begin{bmatrix} 1 & -E_{CZ} & E_{BZ} & E_{XZ} \\ E_{CZ} & 1 & -E_{AZ} & E_{YZ} \\ -E_{BZ} & E_{AZ} & 1 & E_{ZZ} \\ 0 & 0 & 0 & 1 \end{bmatrix} \quad (11) $$

$$ {}^{4}_{5}T = \begin{bmatrix} 1 & 0 & 0 & p_{5x} \\ 0 & 1 & 0 & p_{5y} \\ 0 & 0 & 1 & p_{5z} \\ 0 & 0 & 0 & 1 \end{bmatrix} \quad (12) $$

By transferring to a common machine base coordinate system from two chains, we have:

$$ T = \prod {}^{j}_{k}T_{l} \, {}^{j}_{k}T_{le} \, {}^{j}_{k}T_{m} \, {}^{j}_{k}T_{me} \quad (13) $$

$$ {}^{0}_{3}T = {}^{0}_{1}T \, {}^{1}_{2}T \, {}^{2}_{3}T \quad (14) $$

$$ {}^{0}_{5}T = {}^{0}_{4}T\,{}^{4}_{5}T \tag{15} $$

The volumetric error vector, which describes the relative displacement between the DRI probe and the workpiece surface, is defined as the following:

$$ \begin{bmatrix} E_x \\ E_y \\ E_z \\ 1 \end{bmatrix} = {}^{0}_{3}T \begin{bmatrix} p_{3x} \\ p_{3y} \\ p_{3z} \\ 1 \end{bmatrix} - {}^{0}_{5}T \begin{bmatrix} p_{5x} \\ p_{5y} \\ p_{5z} \\ 1 \end{bmatrix} \tag{16} $$

All the error variables above follow the convention according to the ISO 230-1 [20]. It is time-consuming and unnecessary to measure and model all the error components. More attention should be paid to the influential error components in the sensitive direction because they directly influence the workpiece surface accuracy. In the current work, according to the OMM scanning characteristics and measurement tasks, four kinematic error components in the sensitive *Z* direction of *X* and *C* stages are considered to mainly affect the OMM results. They are *X* axis straightness in the *Z* direction E_{ZX}, squareness error between *X* axis and *C* axis E_{BOC}, *C* axis axial error E_{ZC} and *C* axis tilt error E_{BC} respectively. These four error components are measured, synthesized and employed to generate the kinematic error map in section 3.2.

2.4 Amplification coefficient and linearity error

Due to uncontrolled temperature and humidity in machine tools, environmental variations would cause the response characteristics of high-precision interferometric probe to deviate from a laboratory test. To further analyze and improve the on-machine measurement performance it is necessary to calibrate the response curve of the instrument in the machine tool environment. The linearity error is defined as the maximum deviation of the instrument response curve from the

linear fitted curve where the slope is the amplification coefficient [21]. It is advantageous to employ a multiple step artefact to calibrate the amplification and linearity error of measurement system for the reason that it accounts for the *X*-*Z* squareness error, which behaves as a part of amplification error. According to the turning machine configuration, a radial distributed step height sample is designed, machined, and compared with a calibrated offline instrument. The artefact is designed with four nominal step heights (1 μm, 2 μm, 4 μm and 8 μm) to cover the necessary working range in the *Z* direction, as illustrated in Figure 5. By fitting a first order polynomial curve to the characterization results of the different step heights, the linearity errors and amplification coefficient are consequently derived.

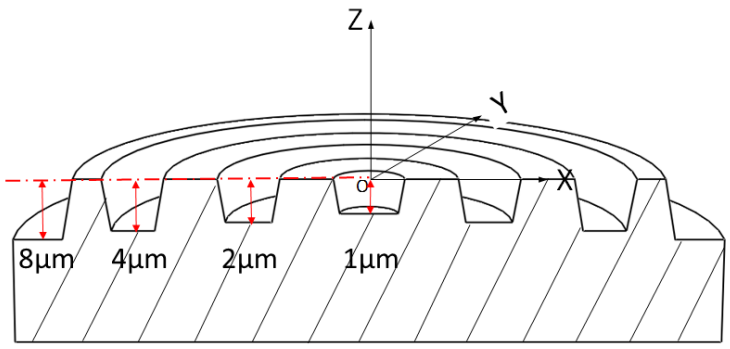

Figure 5 Schematic of radial distributed step artefact

3 Experiments and discussions

To evaluate the proposed calibration process and the performance of DRI on-machine measurement, experimental work and results are presented and discussed in this section.

3.1 On-machine vibration measurement

A calibrated flat standard from NPL Bento Box [22] was employed for static and scanning vibration testing. The vibration measurement results under different test modes are summarized in Table 1. The vibration level is characterized as the root mean square value of the signal.

Table 1 Vibration test results

Probe status	Test Mode	Root mean square RMS /nm
Fixed	**Lab** [13]	0.63
	Static on-machine	2.2
Scanning on-machine	**Multiple radial**	3.5
	Multiple circular	4.4
	Spiral	3.7

The static vibration test was performed when the machine is in static condition, while the scanning vibration test was performed when the machine axes moves simultaneously to measure the sample surface. As presented in the table above, static vibration on the machine is nearly 4 times the DRI internal noise in the laboratory environment, indicating the machine tool environmental effect on the measurement. Furthermore, scanning vibration amplitude is higher than static vibration due to additional vibration arising from the drive units of machine stages. Compared with multiple circular and spiral measurement path, multiple radial path measurement shows the least vibration level of 3.5 nm RMS, which implies the spindle motion induces more vibration than the linear hydrostatic stages.

To reduce the influence of machine kinematic error on the vibration test, six profiles were scanned at a feedrate of 5 mm/min along the radial direction at equally spaced intervals of 30°. The scanning vibration results and frequency analysis are shown respectively in Figure 6 (a) and

Figure 6 (b). As discussed in section 2.2, selection of the DRI sampling frequency should meet the requirement for inspection of the bandwidth of interest on the scale limited surface and avoid signal aliasing. The camera height parameter is used to adjust the sampling frequency of the measurement system. The spectrum analysis in Figure 6 (b) indicates the primary vibration components are less than 100 Hz and the sampling frequency of DRI probe is consequently set to be 200 Hz.

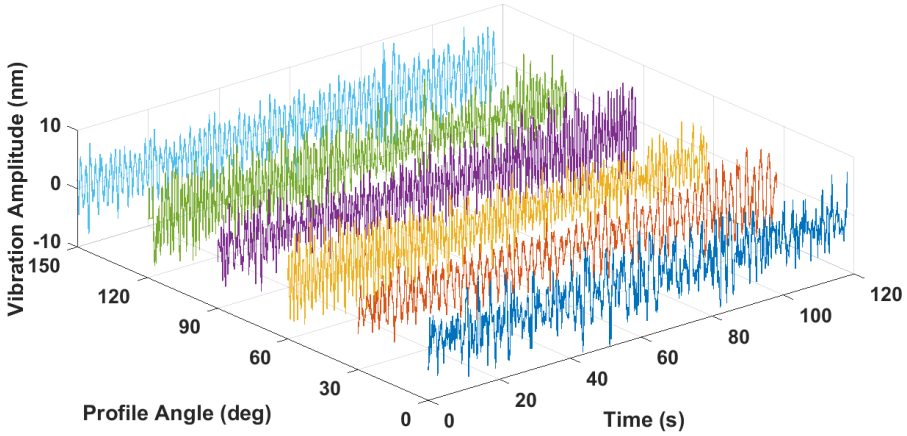

(a) Time domain vibration signal

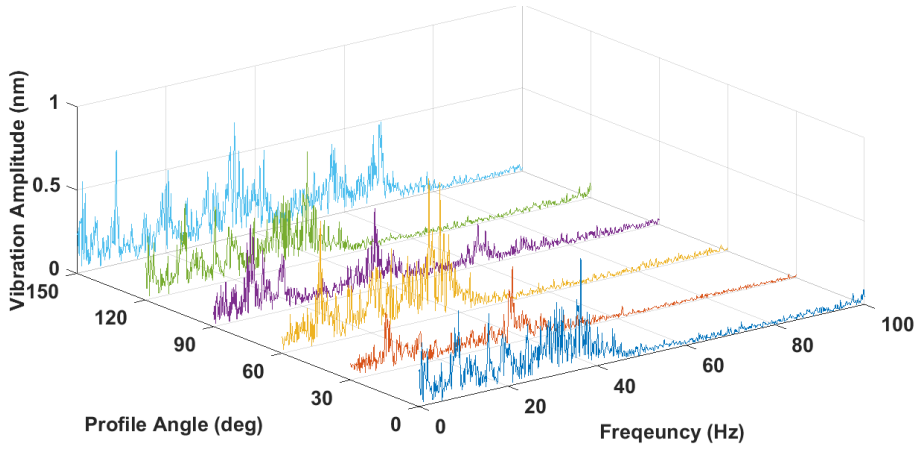

(b) Spectrum analysis of vibration signal

Figure 6 Scanning vibration test

3.2 Kinematic error mapping and compensation

Reversal method has been developed for accurate measurement of part features without reference to an externally calibrated artefact and widely used in ultra-precision machine kinematic error measurement [15, 23]. Four primary error components, including X axis straightness in the Z direction E_{ZX} , squareness error between X axis and C axis E_{BOC}, C axis axial error E_{ZC} and C axis tilt error E_{BC}, were respectively measured using the reversal method. Based on the error measurement and kinematic model established in section 2.3, the machine tool kinematic error illustrated in Figure 7 was numerically mapped and was used for further compensation of on-machine measurement results.

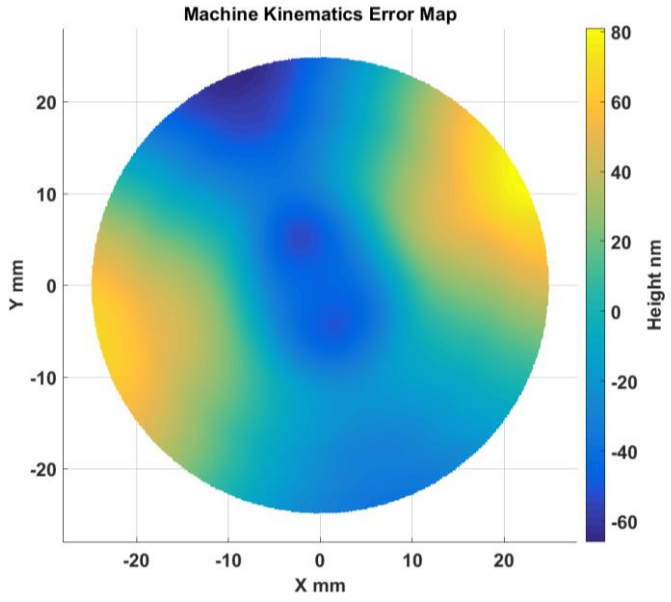

Figure 7 Machine kinematic error map

To validate the generated machine kinematic error map, a commercial optical flat (Edmund optics) was adopted and measured on-machine. Use of a flat surface in the experiment aimed to minimize the effect of linearity error from the DRI probe. The probe was scanned over the sample in a spiral path with C axis rotational speed of 1 rpm and X axis feedrate of 2 mm/min. The flat was also

measured offline on a calibrated Twyman–Green interferometer (Fisba FS10) and this offline result was regarded as the accurate representation of the flat surface form. The measurement results and scanning error map are shown in Figure 8. The scanning error model plot was interpolated from the machine kinematic error map in Figure 7.

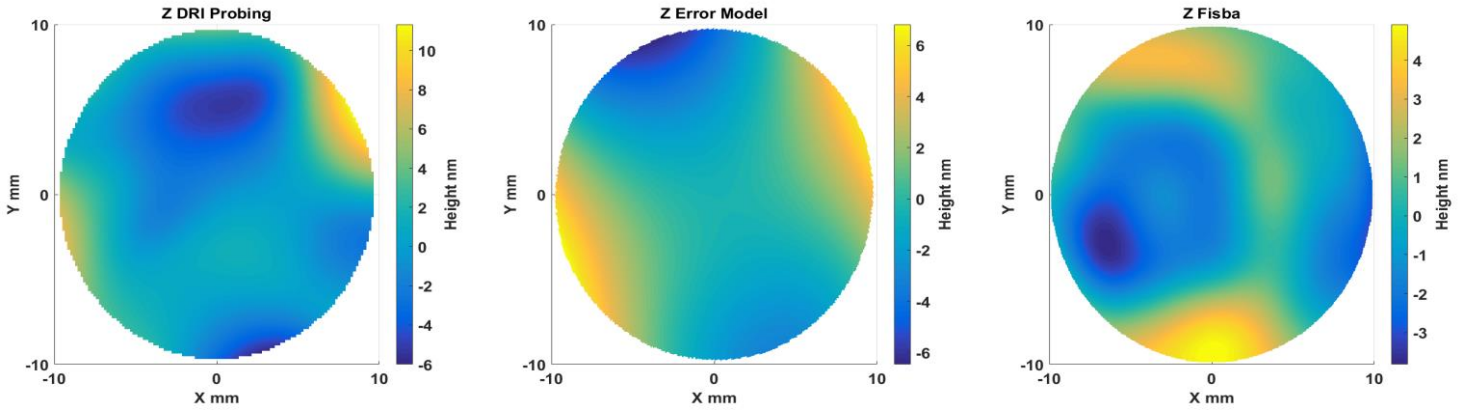

(a) **(b)** **(c)**

Figure 8 DRI measurement (a), scanning error map (b), and Fisba measurement (c) of optical flat

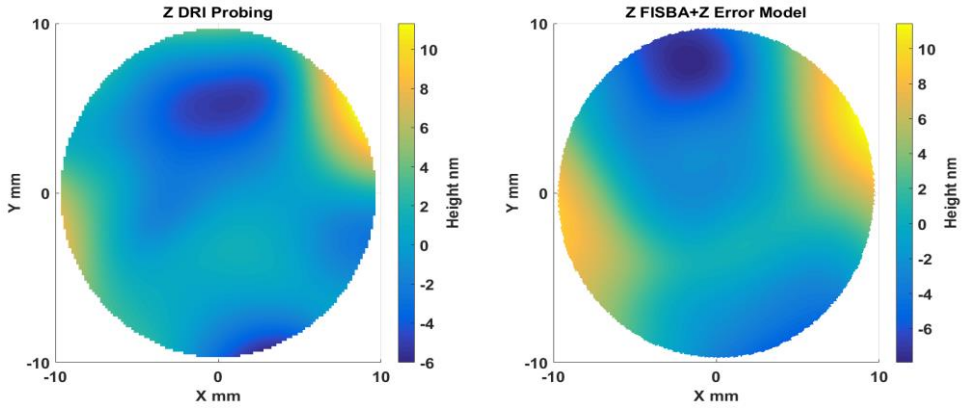

(a) **(b)**

Figure 9 DRI measurement (a) versus combination of scanning error and Fisba measurement (b)

The similarity of two results in Figure 9 indicates that DRI on-machine measurement is the superposition of machine kinematic error and flat form error. With the aid of the machine kinematic error mapping established above, it is possible to compensate for the kinematic errors in

the on-machine probing data. Using this approach the characterized flatness error from on-machine measurement reduced from 17.3 nm to 11.4 nm, compared with results of the calibrated offline measurement of 8.7 nm. It is noted that the offline measurement needs to be aligned to conduct the comparison and the alignment process would inevitably result in some deviation between the two measurements.

3.3 Amplification coefficient and linearity error

Calibration of the amplification coefficient and linearity error in the *Z* direction includes measuring different step heights to study the relationship between the ideal response curve and the instrument response curve. The artefact with 4 step heights (1 μm, 2 μm, 4 μm, and 8 μm respectively) shown in Figure 5 is used for DRI on-machine calibration of amplification coefficient and linearity error. The step height sample was measured on-machine using multiple radial paths. Six measurement profiles are spaced across the surface at equal angles of (30°), as shown in Figure 10. Measurement span was from 10 mm to -10 mm along the radial direction and scanning speed was set at 2 mm/min. The linearity error mainly originates from the DRI single point probing instrument, which is independent of machine tool kinematic error. The pre-mapped machine kinematic error was subtracted from the on-machine measurement data, which was then segmented and mapped onto the workpiece Cartesian coordinate system.

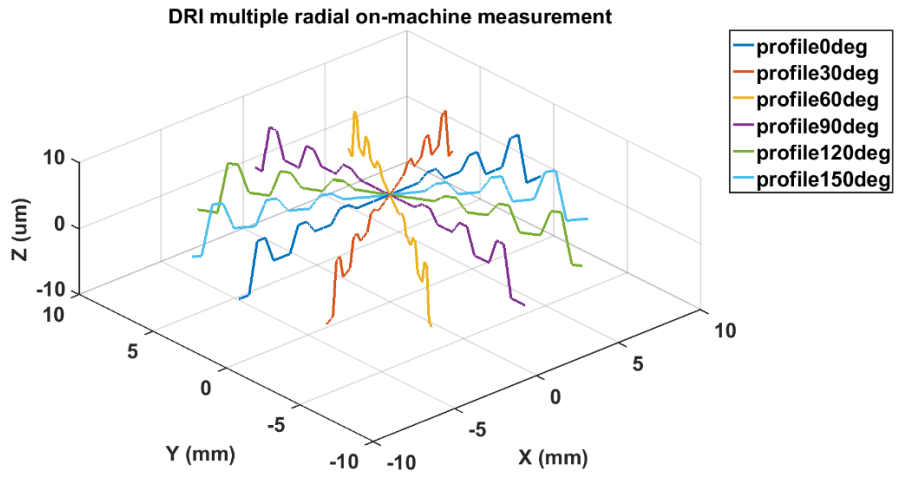

Figure 10 DRI on-machine step artefact measurement

Each extracted radial profile is separated into 4 different step segments, and for each segment the step height is characterized according to ISO 5436 part 1 [24]. Mean step height and repeatability is reported over all radial profiles with 3 repeated measurements. Measurement error δ_{error} is defined as the difference between multiple step height value of on-machine measurement and that of offline calibrated white light interferometer (Talysurf CCI 3000, Taylor Hobson). The CCI result was also employed as the calibrated values to correct the DRI linearity error. The measurement results are summarized in Table 2.

Table 2 Step height measurement results

Design height (µm)	1	2	4	8
DRI on-machine (µm)	0.9969	1.9465	3.9115	7.8199
Talysurf CCI (µm)	1.0011	1.9774	3.9771	7.9128
δ_{error} (µm)	-0.0042	-0.0309	-0.0656	-0.0929

Figure 11 (a) and Figure 11 (b) respectively show the uncorrected and corrected error plot for the step height measurement. The error bars represent the measurement repeatability calculated as the standard deviation of the mean values. After calibration, slope correction coefficient was 1.0123 and the linearity error was reduced from 93 nm to 14 nm.

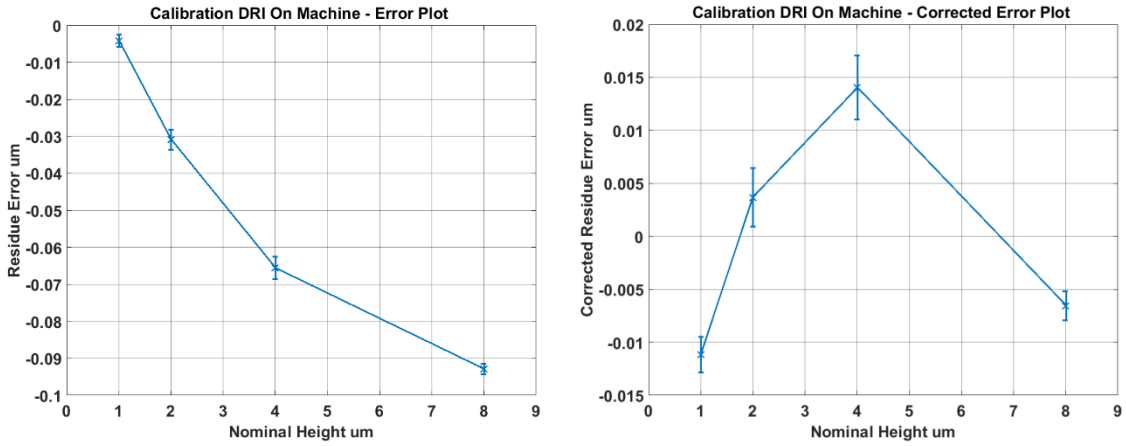

(a) **(b)**

Figure 11 Uncorrected (a) and corrected (b) error plot of the step height measurement

3.4 On-machine measurement experiment

Following the calibration procedure discussed above, two additional samples were measured on the machine. The comparison of OMM results with calibrated offline measurement of the same samples is discussed in this section.

A high precision convex sphere provided by Precitech was scanned in a spiral tool path with *C* axis rotational speed of 1 rpm and *X* axis feedrate of 0.3 mm/min. The sphere surface was nickel plated with stated roughness less than 1 nm. Due to high surface slope, the radius of the measurement area was limited to 1.5 mm. For comparison, offline measurement was performed on a calibrated white light interferometer (Talysurf CCI 3000 with 5X objectives). The measurement results are shown in Figure 12 (a) and Figure 12 (b) respectively. The measured surface was

characterized by radius of curvature, and form error root mean square (RMS) value, summarized in Table 3.

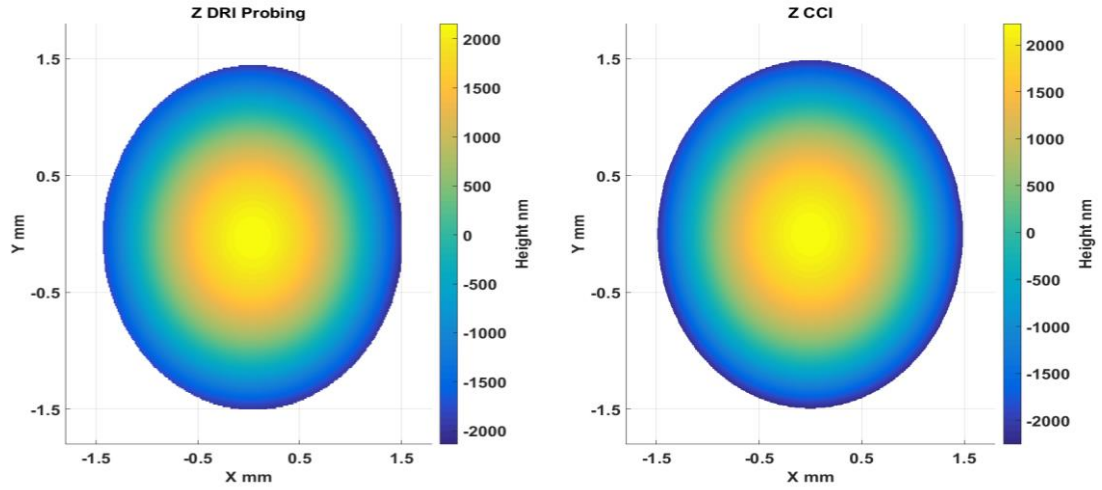

(a) **(b)**

Figure 12 Sphere sample DRI on-machine (a) and CCI measurement (b)

A 2D cosine curve sample ($Z = Acos(2\pi/\lambda X)$) with A =5 μm and λ =2.5 mm was diamond turned and subsequently measured by the DRI on the machine without re-chucking. Profile measurement range was from 4 mm to -4 mm along the radial direction and scanning speed was set to be 2 mm/min. For comparison, offline measurement was carried out on a stylus profilometer (Form Talysurf Series 2 PGI, Taylor Hobson). Results shown in Figure 13 (a) and Figure 13 (b), indicate that DRI on-machine measurement conforms to the PGI offline measurement in terms of form evaluation. The characterization parameters including fitted amplitude, fitted wavelength and form error, were compared and listed in Table 3. Both the measurement were carried out three times for statistical analysis. From the two measurement experiments, it can be seen that the results measured by on-machine measurement system agree well with the calibrated offline measurement results, demonstrating the effectiveness of the calibration process. Although

kinematic error compensation and linearity error correction have been conducted to improve the measurement accuracy, higher measurement error were observed for on-machine measurement of high slope and complex surfaces, resulting from the surface slope effect and non-linearity characteristics of the DRI probe.

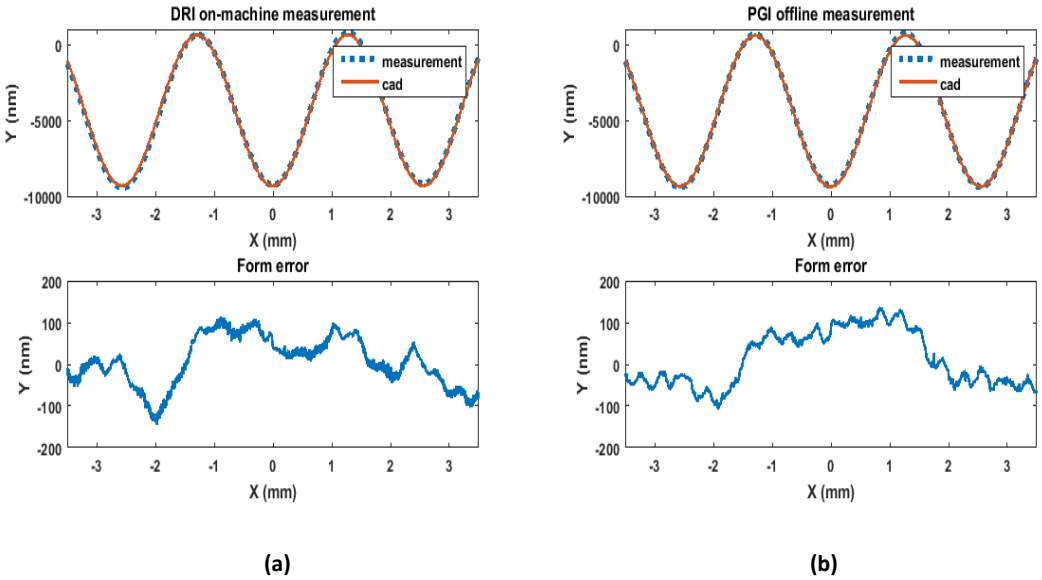

Figure 13 Measurement results and error analysis of DRI on-machine measurement (a) and PGI offline measurement (b)

Table 3 Characterization results of on-machine and offline measurement

Sample	Characterization parameter	DRI on-machine mean (standard deviation)	Offline mean (standard deviation)	Nominal deviation	Deviation (in %)
Convex sphere	**Radius of curvature (mm)**	253.8 (std = 0.056)	246.9 (std < 0.001)	6.9	2.8
	Form error RMS (nm)	10.9 (std = 2.52)	3.7 (std = 0.17)	7.2	194.6
Cosine curve	**Fitted amplitude (µm)**	4.974 (std = 0.0035)	4.982 (std = 0.002)	0.008	1.6
	Fitted frequency (mm^{-1})	0.390 (std = 0.0005)	0.391 (std = 0.0005)	0.001	2.6
	Form error RMS (nm)	58.6 (std = 2.25)	65.7 (std = 1.26)	7.1	10.8

4 Conclusions

This paper presents calibration of an interferometric on-machine probing system for an ultra-precision turning machine. Both theoretical and experimental investigation has been conducted to prove the validity of the proposed calibration methodology and the effectiveness of on-machine measurement. The main conclusions can be drawn as follows:

(1) For on-machine measurement, the machine static and motion vibration tend to induce additional error of measurement results. The frequency decision graph proposed in the present paper can be used to select the proper sampling frequency and scanning parameters.

(2) The optical flat measurement by DRI on-machine and offline Twyman–Green interferometer indicates that the kinematics error compensation can effectively increase the accuracy of the on-machine measurement system.

(3) Calibration method of the response curve for the on-machine measurement instrument is proposed and the linearity error of DRI probe is reduced from 93 nm to 14 nm.

(4) After the calibration process, the results obtained from DRI on-machine measurement system agree well with the results of CCI and PGI offline measurement when measuring a precision sphere and a diamond turned cosine curve surface.

Future work will include the investigation of non-linear characteristics of the interferometric probe, uncertainty analysis of on-machine measurement and measurement result feedback to the machining process to achieve closed loop manufacture.

Acknowledgments

This work is supported by the UK's Engineering and Physical Sciences Research Council (EPSRC) funding (Grant Ref: EP/P006930/1, EP/I033424/1 and EP/K018345/1), European Horizontal project FOF-06-ProSurf (767589) and China Scholarship Council (CSC). The authors appreciate Dr. James Williamson and Dr. Karl Walton for academic discussion of the current paper. The authors also would like to sincerely thank the reviewers for their valuable comments on this work.

References

[1] P. Shore, P. Morantz, Ultra-precision: enabling our future, Philosophical Transactions of the Royal Society A: Mathematical, Physical and Engineering Sciences, 370 (2012) 3993-4014.

[2] L. Blunt, X. Jiang, Advanced techniques for assessment surface topography: development of a basis for 3D surface texture standards" surfstand", Elsevier, 2003.

[3] X. Jiang, Precision surface measurement, Philosophical Transactions of the Royal Society of London A: Mathematical, Physical and Engineering Sciences, 370 (2012) 4089-4114.

[4] X. Jiang, K. Wang, F. Gao, H. Muhamedsalih, Fast surface measurement using wavelength scanning interferometry with compensation of environmental noise, Applied optics, 49 (2010) 2903-2909.

[5] X. Jiang, D. Whitehouse, Miniaturized optical measurement methods for surface nanometrology, CIRP Annals-Manufacturing Technology, 55 (2006) 577-580.

[6] F. Fang, X. Zhang, A. Weckenmann, G. Zhang, C. Evans, Manufacturing and measurement of freeform optics, CIRP Annals-Manufacturing Technology, 62 (2013) 823-846.

[7] R. Leach, C. Giusca, H. Haitjema, C. Evans, X. Jiang, Calibration and verification of areal surface texture measuring instruments, CIRP Annals-Manufacturing Technology, 64 (2015) 797-813.

[8] P.J. de Groot, Progress in the specification of optical instruments for the measurement of surface form and texture, in: SPIE Sensing Technology+ Applications, International Society for Optics and Photonics, 2014, pp. 91100M-91100M-91112.

[9] W.-L. Zhu, S. Yang, B.-F. Ju, J. Jiang, A. Sun, Scanning tunneling microscopy-based on-machine measurement for diamond fly cutting of micro-structured surfaces, Precision Engineering, 43 (2016) 308-314.

[10] W. Gao, J. Aoki, B.-F. Ju, S. Kiyono, Surface profile measurement of a sinusoidal grid using an atomic force microscope on a diamond turning machine, Precision Engineering, 31 (2007) 304-309.

[11] X. Zou, X. Zhao, G. Li, Z. Li, T. Sun, Non-contact on-machine measurement using a chromatic confocal probe for an ultra-precision turning machine, The International Journal of Advanced Manufacturing Technology, (2016) 1-10.

[12] Y. Quinsat, C. Tournier, In situ non-contact measurements of surface roughness, Precision Engineering, 36 (2012) 97-103.

[13] J. Williamson, H. Martin, X. Jiang, High resolution position measurement from dispersed reference interferometry using template matching, Optics Express, 24 (2016) 10103-10114.
[14] R. Wilhelm, R. Hocken, H. Schwenke, Task specific uncertainty in coordinate measurement, CIRP Annals-Manufacturing Technology, 50 (2001) 553-563.
[15] W. Gao, M. Tano, T. Araki, S. Kiyono, C.H. Park, Measurement and compensation of error motions of a diamond turning machine, Precision Engineering, 31 (2007) 310-316.
[16] L.R. Rabiner, B. Gold, Theory and application of digital signal processing, Englewood Cliffs, NJ, Prentice-Hall, Inc., 1975. 777 p., 1 (1975).
[17] R. Ramesh, M. Mannan, A. Poo, Error compensation in machine tools—a review: part I: geometric, cutting-force induced and fixture-dependent errors, International Journal of Machine Tools and Manufacture, 40 (2000) 1235-1256.
[18] A. Okafor, Y.M. Ertekin, Derivation of machine tool error models and error compensation procedure for three axes vertical machining center using rigid body kinematics, International Journal of Machine Tools and Manufacture, 40 (2000) 1199-1213.
[19] C. Raksiri, M. Parnichkun, Geometric and force errors compensation in a 3-axis CNC milling machine, International Journal of Machine Tools and Manufacture, 44 (2004) 1283-1291.
[20] ISO230-1, Test code for machine tools Part 1: Geometric accuracy of machines operating under no-load or quasi-static conditions, (2012).
[21] C.L. Giusca, R.K. Leach, F. Helery, Calibration of the scales of areal surface topography measuring instruments: part 2. Amplification, linearity and squareness, Measurement Science and Technology, 23 (2012) 065005.
[22] R.K. Leach, C.L. Giusca, P. Rubert, A single set of material measures for the calibration of areal surface topography measuring instruments: the NPL Areal Bento Box, Proc. Met. & Props, (2013) 406-413.
[23] C.J. Evans, R.J. Hocken, W.T. Estler, Self-Calibration: Reversal, Redundancy, Error Separation, and 'Absolute Testing', CIRP Annals - Manufacturing Technology, 45 (1996) 617-634.
[24] ISO5436-1, Geometrical product specifications (GPS)—surface texture: profile method; measurement standards—part 1. Material measures (Geneva: International Organization for Standardization), (2000).